Cellular/Molecular

Activity-Dependent Movements of Postsynaptic Scaffolds at Inhibitory Synapses

Cyril Hanus,[1] Marie-Virginie Ehrensperger,[2] and Antoine Triller[1]

[1]Laboratoire de Biologie Cellulaire de la Synapses, Institut National de la Santé et de la Recherche Médicale, and [2]Laboratoire Kastler Brossel, Ecole Normale Supérieure, 75005 Paris, France

Dendritic spines show an activity-dependent cytoskeleton-based remodeling coupled with variations in receptor number and the functional properties of excitatory synapses. In this study, we analyzed the dynamics of gephyrin containing inhibitory postsynaptic scaffolds imaging a Venus::gephyrin (VeGe) chimera in dissociated spinal cord neurons. We provide evidence that the postsynaptic scaffolds at mature synapses display a submicrometric rapid lateral motion and are continuously moving on the dendritic shaft. This dynamic behavior is calcium dependent and is controlled by the cytoskeleton. Minute rearrangement within the gephyrin scaffold as well as the scaffold lateral displacements are F-actin dependent. The lateral movements are counteracted by microtubules. Moreover, the action of the potassium channel blocker 4-aminopyridine and receptor antagonists indicate that the dynamics of postsynaptic gephyrin scaffolds are controlled by synaptic activity.

Key words: **time-lapse imaging; inhibitory synapses; dendritic shaft; cytoskeleton; synaptic activity; calcium**

Introduction

Receptors for neurotransmitters are concentrated at synapses by scaffolding proteins present in postsynaptic differentiations (PSDs). Single-particle imaging of receptor movements in the plasma membrane has shown (1) that receptors are rapidly exchanged between synaptic and extrasynaptic membranes, and (2) that receptors are continuously moving within and out of PSDs with low- and high-diffusion coefficients, respectively (Choquet and Triller, 2003). These results led to the notion that the interactions of receptors with scaffolding proteins are more dynamic than previously expected. Recent evidence indicates that some postsynaptic scaffold proteins at excitatory (Inoue and Okabe, 2003; Huang and El-Husseini, 2005) and inhibitory (Hanus et al., 2004) synapses can be exchanged between the cell surface and intracellular compartments. Using fluorescence recovery after photobleaching assays, the dynamics of scaffolding proteins have been documented on the time scale of a few seconds at excitatory synapses (Okabe et al., 2001). The dynamics of scaffolds at inhibitory synapses have not yet been directly investigated.

The observation of activity-dependent remodeling of dendritic spines on various time scales (seconds, minutes, or hours) has suggested that structural changes could contribute to the regulation of synaptic strength (Carlisle and Kennedy, 2005; Segal, 2005). Electron microscopy studies of excitatory synapses in cultured or acute brain slices have also revealed activity-dependent morphological changes of PSDs and spine architecture (Harris et al., 1992; Toni et al., 1999, 2001; Geinisman et al., 2001; Nicholson et al., 2004). The movements and modifications of the postsynaptic structure have been correlated with changes in the number and turnover of scaffolds (Okabe et al., 1999; Bresler et al., 2001; Dosemeci et al., 2001; Marrs et al., 2001; Ebihara et al., 2003) and receptors (Nusser et al., 1998; Matsuzaki et al., 2001, 2004; Ganeshina et al., 2004) during developmental or plastic modifications of synapses. All of these results have been established for excitatory synapses.

At inhibitory synapses, gephyrin is thought to be the backbone of postsynaptic scaffolds stabilizing the glycine receptor (GlyR) and the main $GABA_A$ receptor ($GABA_AR$). It has been shown that alterations in the cytoskeleton induce changes in the organization of the postsynaptic gephyrin scaffold and alter GlyR stabilization at synapses (Kirsch and Betz, 1995; van Zundert et al., 2002, 2004). This prompted us to examine the dynamic behavior of gephyrin at synapses and its regulation by the cytoskeleton and synaptic activity. For this purpose, we used time-lapse imaging of a Venus::gephyrin (VeGe) chimera in spinal cord neurons. Postsynaptic scaffolds at inhibitory synapses displayed a submicrometric lateral motion around their initial position, on the time scale of seconds. These movements of VeGe clusters were modified after latrunculin, nocodazole, and BAPTA-AM treatments, indicating that the rapid dynamics of inhibitory postsynaptic scaffolds depend on the cytoskeleton and require intracellular calcium. Experiments using potassium channel blocker 4-aminopyridine (4-AP) and glutamate receptor antagonists indicate that movements of inhibitory PSDs are controlled by synaptic activity.

Received Dec. 1, 2005; revised March 1, 2006; accepted March 17, 2006.

C.H. was supported by the Institut de Recherche sur la Moelle Epinière and the Fondation pour la Recherche Médicale. mRFP and Venus encoding plasmids were gifts from Prof. R. Tsien and Prof. K. Mikoshiba, respectively. We thank V. Racine and J.-B. Sibarita (Imaging Facility at the Institut Curie, Paris) for providing the license to use Multidimensional-Images-Analysis software. We thank C. Vannier for providing the untagged-gephyrin plasmid and the anti-gephyrin antiserum and C. Charrier for careful reading and comments on this manuscript.

Correspondence should be addressed to Antoine Triller, Laboratoire de Biologie Cellulaire de la Synapses, Institut National de la Santé et de la Recherche Médicale, Ecole Normale Supérieure, 46 rue d'Ulm, 75005 Paris, France. E-mail: triller@wotan.ens.fr.

DOI:10.1523/JNEUROSCI.5123-05.2006

 0270-6474/06/264586-10$15.00/0

Materials and Methods

DNA constructs. The Venus::gephyrin chimera was obtained by fusing gephyrin (clone p1) (Prior et al., 1992) to the Venus-yellow fluorescent protein (YFP) (Nagai et al., 2002) C terminus via a GlyGlySerLeuGlyGly (GGSLGG) spacer sequence (supplemental Fig. S1, available at www.jneurosci.org as supplemental material). The Venus fragment was amplified by PCR from a plasmid provided by Prof. K. Mikoshiba (Brain Science Institute, RIKEN, Tokyo University, Tokyo, Japan) with primers generating *Bam*HI and *Hind*III sites at the 5′ and 3′ ends, respectively, and was inserted into the pEGFP-N1 expression vector (Clontech, Cambridge, UK) digested by *Bgl*II and *Hind*III. The gephyrin fragment was amplified by PCR from a gephyrin::enhanced green fluorescent protein (eGFP) construct (Meier et al., 2000a) with primers generating *Hind*III and *Not*I sites at the 5′ and 3′ ends, respectively, and was cloned into the previous construct where it replaced the EGFP-encoding sequence.

For expression in mammalian cells, the monomeric red fluorescent protein (mRFP)-encoding sequence was extracted as an *Eco*RI-*Bam*HI fragment from a plasmid provided by Prof. R. Tsien (University of California, San Diego, CA) (pRSTEB-mRFP1) (Campbell et al., 2002) and was cloned into the pEGFP-N1 expression vector digested by *Not*I-*Bam*HI (after blunting of mRFP-*Eco*RI-5′ and pEGFP-N1-*Not*I-3′ ends), where it replaced the EGFP-encoding sequence.

To lower the expression levels driven by this plasmid, three of the four enhancer cassettes of the cytomegalovirus promoter were removed as a *Sna*BI/AseI 300 bp fragment (Boshart et al., 1985).

CDNA structures were checked by sequencing. All endotoxin-free plasmids were prepared using Qiagen (Hilden, Germany) protocols.

Cell culture and transfection. Primary cultures of spinal cord and hippocampal neurons were prepared from embryonic Sprague Dawley rats at days 14 and 18, respectively, as described previously (Meier et al., 2000b; Danglot et al., 2003). Routinely, cells were plated at a density of 5 10^4 (spinal cord) or 2.5 10^4 cells/cm^2 onto 18-mm-diameter glass coverslips (Assistent, Winigor, Germany) coated with 70 μg/ml (spinal cord) or 50 μg/ml (hippocampus) poly-D,L-ornithine (Sigma, St Louis, MO) in 20 mm wells and grown in neurobasal medium supplemented with B27, 2 mM glutamine, and antibiotics (Invitrogen, Cergy Pontoise, France) at 36°C in a 5% CO_2 atmosphere for up to 4 weeks.

Neurons were transfected 8–9 d (spinal cord) or 16 d (hippocampus) after plating using the Lipofectamine2000 method (Invitrogen) according to the protocol of the manufacturer. Cells were usually transfected with 2 μg of plasmid DNA in 20 mm wells. A plasmid molar ratio of Venus::gephyrin to mRFP of four was used in cotransfection experiments.

Live cell imaging and pharmacological treatments. To visualize inhibitory postsynaptic scaffolds at inhibitory synapses, spinal cord neurons [8 d *in vitro* (DIV)] were transfected with Venus::gephyrin. After 48 h of expression, presynaptic terminals were stained with 2 μM *N*-(3-triethylammoniumpropyl)-4-(6-(4-(diethylamino)phenyl)hexatrienyl) pyridinium dibromide (FM4–64) (Invitrogen) in 40 mM KCl-airMEM/B27 (see below) at 37°C for 40 s. Coverslips containing cells were then mounted in a Ludin chamber and incubated in "air-MEM/B27" medium consisting of phenol–red-free minimal essential medium supplemented with 20 mM HEPES, 2 mM glutamine, 1 mM Na-pyruvate, B27 (Invitrogen), and 33 mM glucose (Sigma) and imaged at 36°C under an inverted fluorescence microscope. Cells could be maintained alive for several hours on the microscope stage as checked by Dextran-blue exclusion assays (data not shown). All recordings were performed within a time window of 30 min starting after the FM staining.

Alternatively, to visualize inhibitory postsynaptic scaffolds and dendritic spines, hippocampal neurons (16 DIV) were cotransfected with VeGe and diffuse mRFP and images 48 h after transfection.

Calcium-imaging experiments were done with the Fluo4-AM dye (Invitrogen). Spinal cord neurons (10 DIV) were incubated for 8 min with 0.5 μM Fluo4 in airMEM/B27, extensively washed, and imaged in airMEM/B27 with a set of YFP emission/excitation filters. For similar experiments in transfected cells, neurons were transfected with mRFP after 8 DIV and processed 48 h after transfection.

For pharmacological treatment, cells were preincubated with the drug for different times and then stained with FM4–64 and imaged in the presence of the drug. Drugs were used with the following concentrations and preincubation times: 10 μM nocodazole (Sigma) and 3 μM latrunculin-A (Sigma), 45 min; 30 μM BAPTA-AM (Invitrogen), 30 min; and 50 μM 4-AP, 1 μM tetrodotoxin (TTX), 50 μM CNQX, 50 μM D-AP-5, 1 μM strychnine, 5 μM gabazine, 15 min. Unless otherwise specified, drugs were from Tocris Bioscience (Avonmouth, UK). The solvent DMSO used for latrunculin, nocodazole, and BAPTA-AM had no effect when delivered in the same conditions than the drugs (same final volume and dilution factor).

Immunofluorescence labeling. Immunofluorescence (IF) staining was performed essentially as described previously (Hanus et al., 2004). Briefly, cells were fixed for 15 min at room temperature (RT) in 4% (w/v) paraformaldehyde (Serva Feinbiochemica, Heidelberg, Germany) in PBS, quenched for 20 min at RT with 50 mM NH_4Cl, and permeabilized for 7 min with 0.1% (w/v) Triton X-100 at 4°C. Cells were then incubated for 30 min at RT with 0.25% (w/v) fish gelatin (FG; Sigma) in PBS and incubated with antibodies diluted in 0.1% FG in PBS at RT for 1 h (primary antibodies) or 45 min (secondary antibodies) and washed extensively after each incubation. Coverslips were mounted on slides in Gelmount medium (Biomeda, Foster City, CA), sealed with nail polish, and kept at −20°C.

The various antibodies were used at the following concentrations/dilutions: mouse anti-gephyrin [monoclonal antibody (mAb) 7a; Alexis Biochemicals, San Diego, CA), 1.25 μg/ml; mouse anti-synapsin I (Synaptic Systems, Göttingen, Germany), 1/3000; rabbit anti-synapsin I (Novus Biological, Littletown, CO), 1/2000; mouse anti-α-tubulin (clone DM 1A; Ascites Fluid; Sigma), 1/1000; mouse anti-myc (clone 9E10; Roche Products, Welwyn Garden City, UK), 2 μg/ml; goat anti-rabbit-Texas Red, 1.5 μg/ml; goat anti-mouse-Cy5, 1.5 μg/ml; goat anti-mouse-FITC, 1.5 μg/ml. All secondary antibodies were obtained from Jackson ImmunoResearch (West Grove, PA). For nuclear staining, 50 ng/ml 4′,6′-diamino-2-phenylindole was added to the secondary antibody solution.

Fluorescence picture acquisition and quantitative analysis. Time-lapse sequences of living cells and pictures of fixed cells were acquired under 63× objective lenses on a Leica (Nussloch, Germany) DM-IRB inverted microscope with a CCD camera (Micromax; Princeton Instruments, Trenton, NJ). Acquisition was done in black and white in 12-bit mode using appropriate fluorescence emission/excitation filters. Analysis and quantification were done with MetaMorph software (Princeton Instruments). For illustration and when required, pictures were pseudocolored with MetaMorph or Photoshop (Adobe Systems, San Jose, CA).

Subtractive time lapses used for analysis of fluorescent structure movements. Two frame running subtraction of successive frames showing only moving structures (Fischer et al., 2000) were derived from video time-lapse sequences after removal of the mean out of cells gray value with a homemade routine in MetaMorph.

Detection of fluorescent objects with multidimensional image analysis. Fluorescent clusters were detected with a procedure based on wavelet decomposition (Thery et al., 2005). Briefly, this protocol detects objects based on a comparison of local variations in fluorescence intensities with global noise fluctuations. This process separates small structures with low intensities from large structures with high intensities without thresholding according to absolute fluorescence intensities. We used a multidimensional image analysis (MIA) interface running in MetaMorph. Routinely, fluorescent objects corresponding to gephyrin clusters or synapsin I puncta were detected as fluctuations sevenfold to 20-fold larger than the noise, occurring in the area of two to four pixels (330–660 nm).

Morphological analysis in fixed cells. Sets of neurons compared for quantitation were stained simultaneously. Neurons for imaging were chosen from random areas of each coverslip based on phase contrast showing healthy morphology and the distribution of synapsin puncta showing innervation and imaged using the same exposure time. For each image, regions of interest encompassing 100–200 μm lengths were chosen from two to six dendrites. The cell body regions were excluded from analysis because of high background staining. A custom routine in MetaMorph was used to calculate the proportion of gephyrin clusters at synapses in dendrites. Briefly, binary masks corresponding to gephyrin or

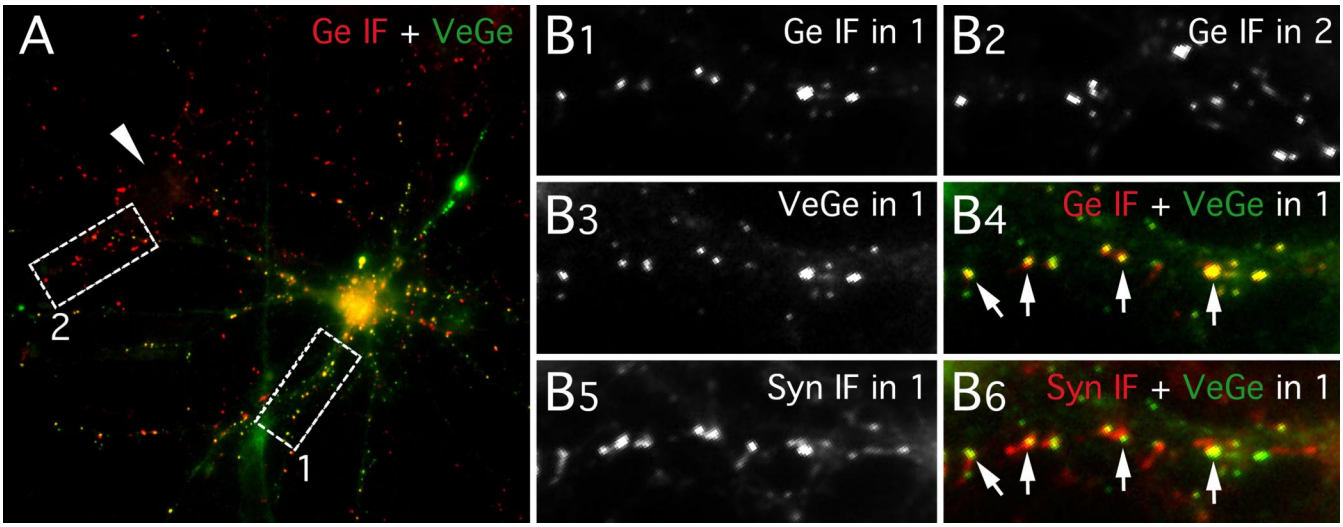

Figure 1. Synaptic localization of Venus::gephyrin. Synapsin I (Syn) and gephyrin (Ge) IF labeling in a spinal cord neuron culture (10 DIV) transfected with VeGe is shown. ***A***, Gephyrin-immunopositive clusters (red) in a transfected neuron (YFP fluorescence, green) and in a nontransfected neuron (arrowhead). ***B***, Higher magnification of areas 1 and 2 (white boxes in ***A***) showing gephyrin-immunopositive clusters in area 1 (***B1***) and area 2 (***B2***), VeGe cluster intrinsic fluorescence in area 1 (***B3***), Syn I-positive presynaptic terminals in area 1 (***B5***), and superimposition of VeGe fluorescence (green) and gephyrin IF (red; ***B4***) or synapsin I IF (red; ***B6***) puncta in area 1. Note (1) that Venus::gephyrin (***A***, ***B3***) and endogenous gephyrin clusters (***A*** and ***B2***) display similar distribution patterns and comparable sizes in a transfected neuron and in a nontransfected neuron, respectively; (2) that all gephyrin IF clusters apposed to presynaptic terminals (arrows in ***B4*** and ***B6***) contain VeGe molecules; and (3) most VeGe clusters are apposed to presynaptic terminals (***B6***).

synapsin I puncta were created by thresholding images segmented with MIA. The percentage of clusters colocalized with presynaptic terminals corresponds to the percentage of thresholded puncta overlapping with the binary mask of the synapsin image.

Fluorescent object tracking and calculation of diffusion coefficients. The VeGe fluorescence mass center was tracked with MIA using a shape recognition algorithm. Values of the mean square displacement (MSD) were calculated from the resulting trajectories with Matlab (The Mathworks S.A.S., Sèvres, France) applying the relation $MSD(ndt) = (N - n)^{-1} \Sigma_{i=1}^{N-n}[(x_{i+n} - x_i)^2 + (y_{i+n} - y_i)^2]dt$ (Saxton, 1997), where x_i and y_i are the coordinates of an object on frame i, N is the total number of steps in the trajectory, dt is the time interval between two successive frames, and ndt is the time interval over which displacement is averaged. The diffusion coefficients were calculated by computing the MSD curves. The trajectories were typically composed of 100 points. The MSD was considered over the first 30 time intervals to avoid large statistical fluctuations (Saxton, 1997). To compare gephyrin cluster dynamics on short and longer time scales in different conditions, two apparent diffusion coefficients D_{ini} and D_{20-30} were derived by fitting the MSD curve with the linear function $MSD(t) = 4\,D_{a\text{-}b} \times t + C_{a\text{-}b}$, between $a = 1$ and $b = 4$, $a = 20$ and $b = 30$, respectively. Because MSD is calculated more precisely for short time scales than for long ones, the fit between $a = 20$ and $b = 30$ was weighted (Qian et al., 1991).

Data were analyzed using Microsoft Excel (Microsoft, Les Ulis, France). Statistical analysis was done using StatView (Abacus Concepts, Berkeley, CA).

Results

We designed a fluorescent gephyrin chimera for live cell imaging experiments in neurons after labeling of active presynaptic terminals with FM4–64. We used the fast maturing and bright modified yellow fluorescent protein "Venus" (Nagai et al., 2002). Its decreased sensitivity toward chloride ions was well suited to the visualization of gephyrin in an environment where local ion concentrations are rapidly changing. Venus::gephyrin was obtained by fusing the Venus-tag to the N terminus of gephyrin (clone p1) (Prior et al., 1992) (supplemental Fig. S1, available at www.jneurosci.org as supplemental material). Most experiments were performed in spinal cord neurons cultured for 10 d, which is after the peak period of inhibitory synaptogenesis in this culture system (Dumoulin et al., 1999).

Synaptic targeting of fluorescent protein-gephyrin chimera

The ability of VeGe to interact with the GlyR was tested in cotransfection experiments in COS-7 cells (Meier et al., 2000a, 2001; Hanus et al., 2004) (supplemental methods, available at www.jneurosci.org as supplemental material). VeGe redistributed to GlyR-containing intracellular membranes and formed submembranous clusters coaggregated with cell-surface receptors when coexpressed with GlyR α1 subunit containing the gephyrin-binding sequence of the β subunit ($\alpha1\beta$gb) (supplemental Fig. S2, available at www.jneurosci.org as supplemental material). The N terminus tagged gephyrin displayed an essentially diffuse distribution pattern when expressed alone (data not shown) or with GlyR α1 subunit (supplemental Fig. S2, available at www.jneurosci.org as supplemental material). This contrasted with gephyrin chimera tagged with GFP at their C terminus, which formed intracellular aggregates (Meier et al., 2000a; Hanus et al., 2004). The distribution patterns of N terminus tagged and untagged gephyrin (in the absence or presence of GlyR) were independent of the variant used (supplemental Fig. S2, available at www.jneurosci.org as supplemental material), indicating that the behavior of VeGe was not a result of the Venus-tag.

To ensure that VeGe was correctly targeted to inhibitory synapses, spinal cord neurons were transfected at 8 DIV and immunoreacted to visualize gephyrin and synapsin I 24 (i.e., 9 DIV) or 48 h (i.e., 10 DIV) after transfection (Fig. 1). Morphological analysis showed that VeGe clusters accumulated at synapses. The size of these clusters, which did not increase with time, was similar to that of endogenous gephyrin clusters in nontransfected cells (Table 1). Forty-eight hours after transfection, most VeGe fluorescent clusters in dendrites (74%) were apposed to synapsin I-immunoreactive (IR) profiles. Conversely, at this stage, ~50% of synapsin I-IR puncta displayed endogenous gephyrin-IR or Venus::gephyrin fluorescence (55 ± 1 and 44 ± 2.5%, respec-

Table 1. Comparison of Venus::gephyrin and endogenous gephyrin clusters in dendrites

	DIV	Clusters area (μm^2)	% of clusters apposed to presynaptic terminals	Cells (n)
Endogenous gephyrin	9	$0.30 \pm 8\ 10^{-3}$	97 ± 0.5	25
	10	$0.29 \pm 6\ 10^{-3}$	97 ± 0.5	27
Venus::gephyrin	9	$0.31 \pm 1\ 10^{-2}$	61 ± 3.5	29
	10	$0.32 \pm 1\ 10^{-2}$	74 ± 3	30

Morphological analysis in spinal cord neurons in cultures transfected at 8 DIV (two independent experiments). Results are expressed as mean per cell ± SEM.

tively), indicating that half of synapsin I-IR profiles were corresponding to inhibitory synapses in this culture system. This is consistent with previous data on endogenous gephyrin (Dumoulin et al., 1999). In transfected cells, most but not all synaptic clusters IR for gephyrin displayed a VeGe-associated fluorescence (Fig. 1). This indicated that inhibitory synapses were not overflowed by overexpressed gephyrin. Alternatively, few synapses may have local exchanges with long time constant. The proportion of clusters apposed to presynaptic terminals was smaller with VeGe than with endogenous gephyrin (Fig. 1, Table 1). This apparent contradiction resulted from the presence of an intracellular pool of gephyrin detected with the VeGe chimera, but which was not well detected with immunofluorescence in nontransfected cells with the mAb7a antibody used in these experiments (Dumoulin et al., 1999; Danglot et al., 2003; Hanus et al., 2004). However, this pool can be visualized unambiguously in nontransfected cells under the electron microscope (Seitanidou et al., 1992; Colin et al., 1996, 1998) or using another commercially available mAb (BD Biosciences, San Diego, CA) (data not shown).

These results indicate that Venus-tagging does not modify the localization of gephyrin at synapses and that the transfected molecules do not create oversize structures. Therefore, VeGe is a reliable probe to visualize inhibitory postsynaptic structures in living neurons, like PSD-95::GFP used to label excitatory PSDs (Craven et al., 1999).

Rapid lateral motion of postsynaptic scaffolds at inhibitory synapses

Approximately 75% of VeGe dendritic clusters were localized at active synapses when imaging living spinal cord neurons stained with FM4–64 (73.4 ± 3.1%; mean ± SEM; $n = 501$ clusters in 12 cells) (Fig. 2*A*,*B*). This was consistent with IF data. Moreover, in dendrites, most of the VeGe clusters close to the cell periphery were apposed to FM4–64-labeled structures.

The movements of VeGe clusters at FM4–64-labeled synapses were analyzed using time-lapse imaging. In the first set of experiments, sequences were acquired at a frequency of one frame per minute during 60–90 min. Although animated by continuous movements, VeGe clusters apposed to FM4–64 boutons remained in the close vicinity of their initial position within 1 h periods (maximum lateral displacements were on the order of 1 μm; data not shown). Most VeGe synaptic clusters therefore corresponded to "stable" synapses. Some VeGe clusters not apposed to FM4–64-labeled boutons were also stable. As suggested by IF data (Fig. 1), these clusters were likely to be in front of synaptic boutons not active during the incubation with the FM4–64 dye or may have corresponded to extrasynaptic clusters of gephyrin (Dumoulin et al., 1999).

The rapid movements of VeGe clusters at synapses were monitored using time-lapse sequences of YFP fluorescence digitized at 1 Hz for 100 s periods (Fig. 2*A–C*). For this analysis, distinct VeGe clusters were classified into two classes according to their motility and relationship to FM4–64-labeled boutons (Fig. 2*B*). The first group corresponded to small clusters (diameter, ~0.3 μm) within the cytoplasm and had a rather linear motion with high velocity (on the order of 0.5 μm/s) (movie 1, available at www.jneurosci.org as supplemental material). These objects often paused near larger VeGe clusters themselves apposed to FM4–64 boutons. These small clusters likely correspond to intracellular gephyrin carriers traveling along microtubules (Hanus et al., 2004; Maas et al., 2006). The second class of objects corresponded to VeGe clusters localized at synapses. They were larger (diameter, ~0.6 μm) and apparently less mobile than the previous ones. After close inspection, these synaptic clusters were moving rapidly over short distances (0.5–1 μm) and seemed to be oscillating around a fixed tether (movie 1, available at www.jneurosci.org as supplemental material). The latter movements could be objectified using a subtractive image-processing method allowing selective detection of fluorescence displacements (Fischer et al., 2000). Two-frame subtraction sequences were derived from time lapses, and projection of the resulting pictures indicated that VeGe synaptic clusters were moving (Fig. 2*C*). This "dancing" behavior can be compared with that seen for dendritic spines, which has been extensively characterized in hippocampal neurons (Matus, 2000). For this purpose, we monitored the dynamics of VeGe clusters in hippocampal neurons in parallel to the dynamics of dendritic spines. Time-lapse sequences of VeGe and mRFP fluorescence were digitized at 0.065 Hz for 5 min periods (Fig. 2*D–F*) (movie 2, available at www.jneurosci.org as supplemental material). Projection of two-frame subtraction sequences derived from time lapses showed a large signal associated with dendritic spines and for clusters at the shaft for mRFP (Fig. 2*E*) and VeGe (Fig. 2*F*), respectively. Therefore, as was found in spinal cord neurons, VeGe clusters on the dendritic shaft exhibited rapid small-scale lateral motion with an amplitude comparable with that of the rapid morphing of dendritic spines. Interestingly, the dendritic shaft remained with a weak homogeneous signal indicating that it was not submitted to changes in shape. The strong contrast between gephyrin cluster and dendritic shaft signals (Fig. 2*E*,*F*) indicates that their movements are independent. These movements of VeGe clusters in hippocampal neurons indicate that the lateral displacement of postsynaptic scaffolds at inhibitory synapses is not a specific feature of spinal cord neurons and that postsynaptic scaffolds are dynamic, whether or not they are localized on protrusive membranes.

Effects of cytoskeleton disruption and intracellular calcium buffering on inhibitory postsynaptic scaffold dynamics

The motion of VeGe synaptic clusters was compared in spinal cord neurons in control conditions and in the presence of latrunculin, nocodazole, or BATPA-AM. Regulation of cytoskeleton dynamics, more especially that of F-actin, as well as variations in intracellular calcium concentration are key regulators of dendritic spine motion (Oertner and Matus, 2005). For our experiments, VeGe clusters in time-lapse sequences were individualized using image wavelet decomposition (see Materials and Methods) (Fig. 3*A*) (movie 3, available at www.jneurosci.org as supplemental material). The mass centers of clusters apposed to FM4–64 puncta were tracked individually, and the resulting trajectories (Fig. 3*B*) were used to determine the instantaneous velocity of clusters. Variations in cluster instantaneous velocities as a function of time (Fig. 3*C*) showed that clusters, even when close one to each other, were not moving synchronously. This is emphasized in the inset where the amplitudes have been normalized.

This further supports the notion that the movements of gephyrin postsynaptic clusters and that of the dendritic shaft are independent. Comparison of the instantaneous velocity fluctuations under control conditions or after treatment with latrunculin showed that gephyrin cluster dynamics were decreased after F-actin disruption. Instantaneous velocities could be used to compare postsynaptic gephyrin dynamics in various conditions, but large fluctuations with time and between clusters did not facilitate analysis. Therefore, the MSD as a function of time [MSD = $f(t)$] of the mass center of the fluorescent clusters was preferred (Fig. 4). Briefly, the MSD = $f(t)$ function was calculated by averaging the square displacement of objects within trajectory stretches corresponding to increasing time-step sizes (see Materials and Methods). A major advantage of this analysis is that it distinguishes between different types of displacements (free, constrained, or directed diffusions) (Saxton, 1993, 1997) that cannot be detected when simply comparing instantaneous velocity variations with time. Another advantage of the MSD = $f(t)$ function is that it allows to derive diffusion coefficients that can be used to compare object dynamics on different time scales (Kusumi et al., 2005).

The dynamic behaviors of synaptic clusters depended on the experimental conditions tested. MSD values were globally increased in cells treated with nocodazole and decreased in cells treated with latrunculin and BAPTA-AM, compared with values found in control cells (Fig. 4*A*). Rapid movements of the mass center of the fluorescent clusters (short time intervals) are likely to reflect minute rearrangement within clusters and therefore a change in the position of the mass center. Larger movements of the entire clusters are better estimated by diffusion measurement over longer timer intervals (Saxton, 1993, 1997; Meier et al., 2001). Therefore, diffusion coefficients were derived from MSD = $f(t)$ plots at various time intervals (Fig. 4*B*,*C*), and integrated diffusion coefficients D_{ini}, and D_{20-30} were derived for 1–4 and 20–30 s intervals, respectively (see Materials and Methods). Dynamics of VeGe synaptic clusters with the different treatments were compared using pooled diffusion coefficient distributions (Fig. 4*B*) and mean median values of diffusion coefficients per cell (Fig. 4*C*). D_{ini} distribution was shifted toward lower values in cells treated with latrunculin and to a smaller extent in cells treated with BAPTA-AM, compared with distribution in control and nocodazole-treated cells (Fig. 4*B*). This was accentuated for the 20–30 s intervals: D_{20-30} values were shifted toward lower values in cells treated with latrunculin and BAPTA-AM and toward higher values in cells exposed to nocodazole, compared with control cells. These effects were also seen when comparing median

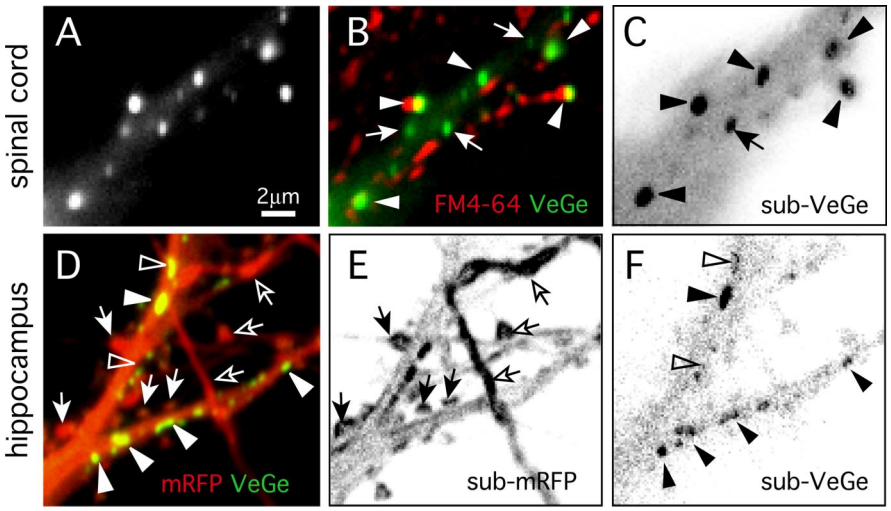

Figure 2. Movements of postsynaptic scaffolds at inhibitory synapses. Characterization of VeGe synaptic cluster dynamics in cultured spinal cord (10 DIV; ***A–C***) and hippocampal (18 DIV; ***D–F***) neurons is shown. ***A***, VeGe clusters in a spinal cord neuron proximal dendrite. ***B***, Same field as in ***A*** with VeGe in green and FM4–64 staining in red. VeGe synaptic and extrasynaptic clusters (arrowheads and arrows, respectively) are identified according to their position relative to FM4–64 puncta. ***C***, Two-frame running subtraction projection (see Materials and Methods for details) corresponding to a time-lapse sequence of the field shown in ***A*** and ***B*** (101 frames; $dt = 1$ s). The signal (black) corresponds to fluorescent object displacements (inverted contrast). Note the strong signal associated with large synaptic (arrowheads) and some smaller extrasynaptic (arrow) clusters showing that these objects were moving over short distances around their initial position. ***D***, Visualization of dendritic spines and inhibitory synapses in a hippocampal neuron (18 DIV) cotransfected with mRFP and VeGe. ***E***, ***F***, Two-frame running subtraction projection of mRFP (***E***) and VeGe (***F***) time-lapse sequences in the field shown in ***D*** (50 frames; $dt = 10$ s). Note the strong signal associated with dendritic spines (arrows) and VeGe clusters (arrowheads). Displacement of mRFP aggregates in some neurons gives a strong signal in axons (open arrows). Note that some VeGe clusters are less dynamic than others (open arrowheads).

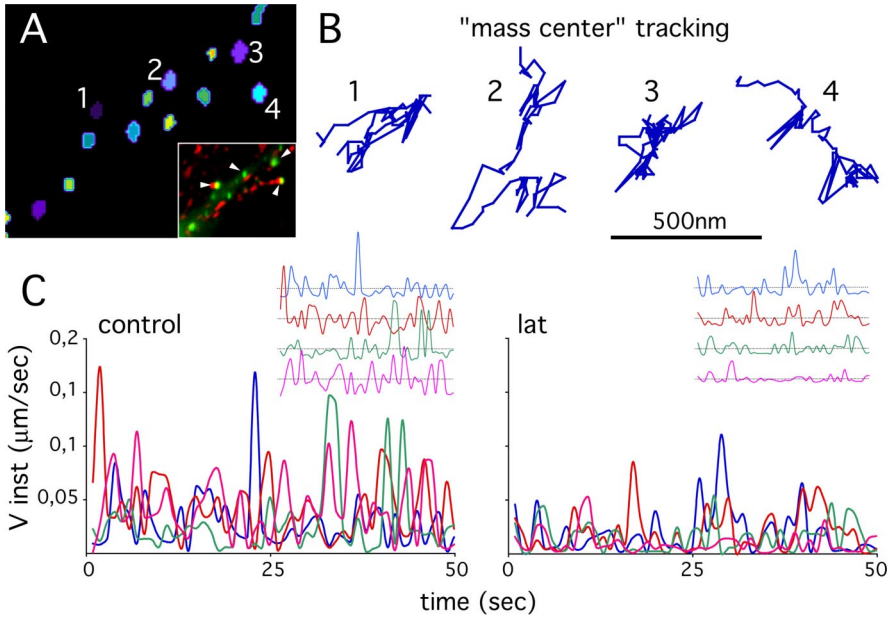

Figure 3. Velocities of VeGe synaptic clusters. ***A***, Segmentation and individualization of VeGe synaptic clusters (1–4) in the field shown in the inset (arrowheads; VeGe in green, FM4–64 staining in red; same field as in Fig. 2*A–C*). Individual clusters are identified by a color code. ***B***, Trajectory of the fluorescence "mass center" of the four synaptic clusters highlighted in ***D***. ***C***, Instantaneous velocities (V_{inst}) as a function of time of four VeGe synaptic clusters in a control cell (same clusters as in ***A*** and ***B***) and in a cell exposed to 3 μM latrunculin. Insets, Fluctuations with time of V_{inst} relative to average value on each trajectory. Note the reduced dynamics of VeGe clusters after latrunculin treatment.

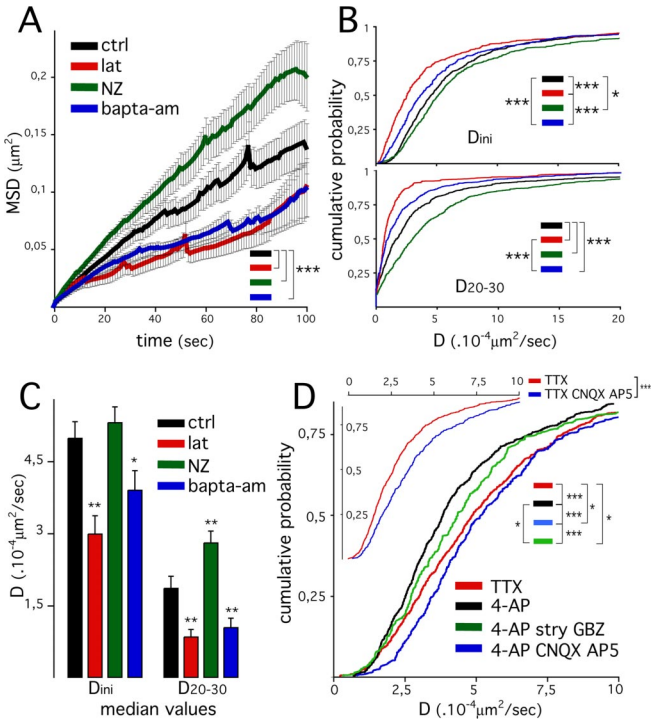

Figure 4. Dynamics of inhibitory postsynaptic scaffolds, cytoskeleton, intracellular calcium, and synaptic activity. ***A***, Averaged mean square displacement as a function of time in spinal cord neurons (10 DIV) in control conditions (ctrl; black) and during treatment with 3 μM latrunculin (lat; red), 10 μM nocodazole (NZ; green), or 30 μM BAPTA-AM (blue). Results are expressed as means ± SEM (31, 16, 21, and 22 cells were analyzed for ctrl, lat, NZ, and BAPTA-AM, respectively; 3 experiments; Kolmogorov–Smirnov test, $***p < 10^{-3}$). ***B***, ***C***, Comparison of diffusion coefficients derived from MSD = $f(t)$ plots for time intervals between 1–4 s (D_{ini}) and 20–30 s (D_{20-30}). ***B***, Distribution of D_{ini} (bottom panel) and D_{20-30} (bottom panel) values (630, 331, 551, and 373 clusters were analyzed for ctrl, lat, NZ, and BAPTA-AM, respectively). ***C***, Mean diffusion coefficients median in individual cells (mean ± SEM; cf. effectives in ***A***; ANOVA, PLSD test, $***p < 10^{-3}$; $**p < 10^{-2}$; $*p < 0.05$). Same colors as in ***A***. ***D***, Comparison of diffusion coefficient (D_{ini}) distribution in cells treated with TTX (red) and in cells treated with 50 μM 4-AP (black), 4-AP plus 50 μM AP-5/CNQX (blue), or 4-AP plus 1 μM strychnine (stry) plus 3 μM gabazine (GBZ) (green) (782, 443, 369, and 906 clusters from 19, 20, 21, and 18 cells were analyzed for 4-AP, 4-AP/AP-V/CNQX, 4-AP/stry/Gbz, and TTX, respectively; 2 and 4 experiments were done with 4-AP, 4-AP/AP-V/CNQX, 4-AP/stry/Gbz, TTX, and 4-AP,TTX, respectively; Kolmogorov–Smirnov test, $***p < 10^{-3}$, $**p < 10^{-2}$). Inset, Comparison of diffusion coefficients (D_{ini}) distribution in cells treated with TTX (red) or TTX plus CNQX and AP-5 (blue) (795 and 544 clusters, in 30 and 26 cells, were analyzed for TTX and TTX plus CNQX plus AP-5, respectively; 2 experiments, independent of those presented in the main graphic; Kolmogorov–Smirnov test, $***p < 10^{-3}$).

values per cell: D_{ini} median was decreased in cells treated with latrunculin or BAPTA-AM but was not modified in cells exposed to nocodazole, but although D_{20-30} median was decreased by latrunculin and BAPTA-AM, it was increased by nocodazole. Importantly, D_{ini} values calculated for clusters with reduced dynamics (i.e., with latrunculin or BAPTA-AM treatment) were always higher (× 5.4) than that calculated in fixed cells (supplemental Fig. S3, available at www.jneurosci.org as supplemental material). Therefore, the lowest diffusion coefficients derived from living cells were well above the resolution limit of our assay.

The effect of F-actin and nocodazole on gephyrin synaptic cluster movements on short and longer time scales suggests that these two cytoskeleton components make different and opposite contributions to postsynaptic scaffold dynamics at inhibitory synapses. Furthermore, whatever the time scale, the movements of VeGe synaptic clusters were calcium dependent. Our results indicate the following: (1) rapid movements of gephyrin molecules within clusters at the postsynaptic membrane rely on F-actin but do not involve nocodazole-sensitive microtubules; and (2) dynamics of postsynaptic structures on longer time scales, which likely correspond to lateral displacements of the entire postsynaptic structure, also rely on F-actin but are counteracted by nocodazole-sensitive microtubules. In good agreement with a role of F-actin in this process, phalloidin staining and IF labeling for synapsin I in 10 DIV spinal cord neurons revealed the presence of F-actin patches at synapses on the dendritic shaft (data not shown).

Enhanced synaptic activity decreases the lateral motion of the inhibitory postsynaptic scaffolds

The notion that the morphing of dendritic spines relies on F-actin dynamics and is tuned by the synaptic activity has been documented extensively in dendritic spines (Oertner and Matus, 2005). Experiments similar to those presented above were performed to analyze the effect of synaptic activity on gephyrin dynamics at synapses.

In preliminary experiments, calcium imaging was used to verify the existence of a spontaneous synaptic activity in transfected spinal cord neurons. Cells transfected with diffuse mRFP were loaded with Fluo4. Fifty second stream sequences of Fluo4 fluorescence in fields containing transfected cells were digitized at 10 Hz. In basal conditions, rapid calcium fluctuations were observed in transfected cells (supplemental Fig. S4, available at www.jneurosci.org as supplemental material). These oscillations were most likely linked to spontaneous synaptic activity, because they were abolished by the sodium channel blocker TTX and enhanced by the potassium channel blocker 4-AP (movie 4, available at www.jneurosci.org as supplemental material). These calcium fluctuations were variable from one cell to another. To minimize intrinsic fluctuation within an experimental session, a situation with maximum synaptic activity (i.e., treatment with 4-AP) was preferred for controls. 4-AP induced an important and rapid loss of FM4–64 staining (data not shown), therefore providing a good control of the specificity of this staining for visualization of active synapses. However, FM4–64 could no longer be used to identify synaptic boutons. Therefore, VeGe clusters to be analyzed were identified by means of morphological criteria, such as shape, size, and localization at the dendrite periphery. To compare the dynamics of postsynaptic structures with those of "individual" GlyR at synapses as measured by single-particle tracking, which are relatively rapid (diffusion coefficients in the order of $\sim 10^{-2}$ $\mu m^2/s$) (Dahan et al., 2003), we focused our analysis on VeGe cluster lateral motion on short time scales (1–4 s). Diffusion coefficient (D_{ini}) distribution was shifted toward higher values in cells exposed to TTX compared with cells treated with 4-AP (Fig. 4*D*). This indicates that axonal firing slows down the lateral movements of gephyrin synaptic clusters. Distributions of diffusion coefficients derived for longer time intervals (D_{1-30} and D_{20-30}) were not significantly different (data not shown). This indicates that on a short time scale, axon firing and synaptic activity reduce the lateral dynamics of postsynaptic inhibitory scaffolds.

To determine whether the decrease in gephyrin dynamics induced by 4-AP was directly mediated by fast synaptic transmission, similar experiments were performed with drugs blocking neurotransmitter receptors present at synapses in cultured spinal cord neurons (O'Brien et al., 1997, 1998; Levi et al., 1999). Interestingly, the effect of 4-AP was reversed by the addition of the glutamate ionotropic receptor blockers CNQX and AP-5 (Fig. 4*D*). TTX was not as efficient as AP-5–CNQX (added to 4-AP),

suggesting that spontaneous release of neurotransmitter already reduced the dynamics of VeGe clusters in the presence of TTX. This hypothesis is supported by the fact that CNQX–AP-5 and TTX effects were additive (Fig. 4*D*, inset). The distribution of D_{ini} values with 4-AP was slightly shifted toward higher values by the addition of strychnine and gabazine, specific blockers for glycine and $GABA_A$ receptors, respectively. Notably, this shift was smaller than that after CNQX/AP-5 treatment.

These data indicate that enhancement of axonal firing reduces the rapid dynamics of gephyrin synaptic clusters. The implication of postsynaptic receptors in this process emphasizes the notion that synaptic activity directly controls the dynamics of gephyrin at synapses.

Discussion

Movements of gephyrin synaptic clusters on the dendritic shaft were found in spinal cord and in hippocampal neurons. The latter movements occurred with an amplitude similar to that of the rapid morphing of dendritic spines. Therefore, our data establish that all postsynaptic structures display a rapid dynamic behavior whether or not they are localized on spines. These short time scale movements of synaptic clusters were much faster than the global movements of the entire dendrite. Moreover, synaptic VeGe clusters were not moving synchronously, indicating that their lateral motion was attributable to local constraints on individual synapses and not to changes affecting global cell morphology.

Tracking of the fluorescence mass center of VeGe synaptic clusters and analysis of resulting trajectories allowed us to identify fast and slow components of postsynaptic scaffold motion. These likely correspond to rearrangement within postsynaptic clusters and to lateral displacements of entire clusters, respectively. The effects of latrunculin and nocodazole on synaptic cluster diffusion analyzed on short ($<$5 s, "rapid component") and longer ($>$10 s, "slow component") time scales indicated that F-actin and microtubules make different contributions to inhibitory postsynaptic scaffold dynamics. Minute rearrangements within postsynaptic clusters were diminished after F-actin disruption but not by that of nocodazole-sensitive microtubules. In contrast, the dynamics of postsynaptic clusters on longer time scales were also decreased by F-actin depolymerization but were increased by that of microtubules. This suggests that the global dynamics of inhibitory PSDs rely on F-actin and that their lateral displacement is counteracted by microtubules. Indeed, previous data that have shown that F-actin and microtubule disruption have opposite effects on the morphology of gephyrin synaptic clusters (Kirsch and Betz, 1995). More precisely, disruption of F-actin leads to a packing of postsynaptic gephyrin into clusters of increased density, whereas disruption of microtubules induces opposite effects. The implication of microtubules in this process contrasts with what has been described for spine dynamics, which are microtubule independent (Halpain, 2000). This difference may result from the localization of inhibitory synapses on the dendritic shaft, which contains microtubules and F-actin, whereas spines contain only F-actin (Dillon and Goda, 2005). Different lines of evidence suggest that excitatory synapses on spines or the shaft display distinct composition/organization and properties (O'Brien et al., 1997; Allison et al., 1998; Lissin et al., 1998; Rao et al., 1998; McBain et al., 1999; Zhang et al., 1999). Importantly, mechanisms accounting for the aggregation/stabilization of glutamate receptors at these synapses are different (Allison et al., 1998, 2000; Mi et al., 2002). Although microtubules are not responsible for the stabilization of excitatory receptors at shaft synapses, it would be interesting to analyze the relative contributions of F-actin and microtubules to the morphological dynamics of these synapses.

Numerous molecules among gephyrin-binding partners are physically or functionally linked to the cytoskeleton (supplemental Fig. S5, available at www.jneurosci.org as supplemental material). These molecules are likely to be involved in the dynamics of postsynaptic scaffolds and in the regulation GlyR diffusion at inhibitory synapses.

An important issue of the present study is that it allows a comparison of receptor dynamics at synapses with that of postsynaptic scaffolds. Notably, the global lateral motion of postsynaptic gephyrin measured over seconds (mean, $D \sim 7.1\ 10^{-4}\ \mu m^2/s$) is slower than the diffusion of synaptic receptors as measured by single-particle tracking (mean, $D \sim 1.5\ 10^{-2}\ \mu m^2/s$) (Dahan et al., 2003). Although we cannot exclude that some gephyrin molecules bound to GlyR (likely corresponding to "slow" synaptic receptors; mean, $D \sim 1\ 10^{-3}\ \mu m^2/s$) (Dahan et al., 2003) may diffuse as fast as receptors, the diffusion of receptors and the lateral motion of postsynaptic scaffolds are two distinct types of movements within synapses. Therefore, the decreased diffusion of receptors at synapses reflects their "confinement" (Choquet and Triller, 2003) by postsynaptic scaffolds that are themselves moving on longer time scales, a concept that was hypothesized when analyzing the shape of MSD curves (Triller and Choquet, 2005).

We also found that synaptic activity controls the dynamics of postsynaptic scaffolds at inhibitory synapses. Enhancement of axon firing after 4-AP treatment reduced the movements of inhibitory postsynaptic scaffolds. This effect of 4-AP was directly caused by an increased synaptic transmission, because excitatory receptor antagonists reversed it. Finally, inhibitory receptor antagonists also limited the effect of 4-AP but induced a smaller decrease in gephyrin dynamics than that produced by glutamate receptor antagonists. We cannot formally exclude that global modifications of network activity may have contributed to the observed effects, because excitatory synapses also control inhibitory interneuron firing rate. However, our quantitative data favor the notion that the lateral dynamics of inhibitory synapses are directly controlled by the activity of excitatory synapses and, to a lesser extent, by that of inhibitory ones. This is consistent with a recent study showing that excitatory cholinergic inputs affect the morphological and functional properties of inhibitory synapses in Renshaw cells of the spinal cord (Gonzalez-Forero et al., 2005). Regulation of postsynaptic structure motility by synaptic activity is well documented for dendritic spines. The actin-driven high motility of dendritic spines (Matus, 2000) is decreased by calcium influx through glutamate receptors and calcium channels (Fischer et al., 2000). Interestingly, many proteins regulating F-actin are calcium dependent and might transduce intracellular calcium levels into changes in spine dynamics (Oertner and Matus, 2005). Among them, profilin and gelsolin are known to regulate F-actin in spines (Star et al., 2002; Ackermann and Matus, 2003). Notably, several actin regulators also control microtubule dynamics (Watanabe et al., 2005). Some molecules involved in these signaling pathways (e.g., the Cdc42 GTPase activating protein IQGAP1) are regulated by calcium (Briggs and Sacks, 2003) and may therefore be important for the regulation of F-actin and microtubules at shaft synapses.

The decreased and increased gephyrin dynamics with BAPTA-AM and 4-AP/CNQX/AP-5 treatment, respectively, are apparently contradictory, because NMDA receptor (NMDAR) and AMPA receptor activations are expected to increase intracel-

lular calcium concentration. Nevertheless, in good agreement with previous data (Kirsch and Betz, 1998), the effect of BAPTA-AM indicates that the dynamics of inhibitory postsynaptic scaffolds are calcium dependent. Our results contrast with the lowered dynamics of dendritic spines after calcium influx via NMDARs and/or low voltage calcium channels (Oertner and Matus, 2005). This discrepancy may be because of the extrasynaptic location of NMDAR in our culture system (O'Brien et al., 1997, 1998) and/or nonlinear effects of intracellular calcium concentrations. Opposite effects of calcium at different concentrations have been found in several biological processes such as long-term potentiation (LTP)/long-term depression (LTD) (Rose and Konnerth, 2001), axon growth cone turning (Zheng, 2000), and apoptosis induction (Berridge et al., 1998). Importantly, rapid calcium influx through plasma membrane channels and calcium release from intracellular stores can have different effects, as well as local versus global activation of synaptic activity (Rose and Konnerth, 2001; Kennedy et al., 2005). Unraveling the respective contribution of extracellular calcium and intracellular calcium stores in the control of inhibitory PSD dynamics, in relation with local synaptic activity, will be important to understand the functional interactions between excitatory and inhibitory synapses.

Spine motility and regulation by synaptic activity are associated with rapid F-actin dynamics, and high levels of actin turnover (Star et al., 2002) and polymerization/depolymerization fluctuations (Okamoto et al., 2004) are seen at synapses. The intrinsic dynamics of postsynaptic structure and that of dendritic spines may be different, even if tightly interconnected. Our data suggest that postsynaptic scaffolds themselves, even on dendritic shafts, display a rapid lateral motion that relies on the cytoskeleton and intracellular calcium. Functionally, stimulation patterns triggering LTP and LTD affect both glutamatergic synapse responses and the morphology of dendritic spines (Halpain, 2000; Oertner and Matus, 2005). Thus, F-actin and functional plasticity of synapses are linked (Kim and Lisman, 1999; Krucker et al., 2000; Zhou et al., 2001). The notion that synaptic activity controls the cytoskeleton to tune the number of receptors at synapses might also hold at inhibitory synapses. Previous data have established that F-actin and microtubule depolymerization modify the organization of postsynaptic gephyrin scaffolds (Kirsch and Betz, 1995). Furthermore, microtubules (van Zundert et al., 2002, 2004) and F-actin disruptions (Kirsch and Betz, 1995) alter GlyR stabilization at synapses, indicating that the cytoskeleton controls the number of inhibitory receptors at synapses. However, the number of synaptic $GABA_AR$ clusters is not modified in these conditions (Allison et al., 1998, 2000) (but see Meyer et al., 2000; Petrini et al., 2003). It should be noted that cell types and quantification methods used in these studies differ.

The question of how regulation of receptor numbers at synapses is connected with postsynaptic structure dynamics is still not fully understood. Interestingly, a recent study provided evidence that membrane proteins diffuse faster in immobile spines (as observed for glutamate application or F-actin disruption) than in mobile spines (Richards et al., 2004). This points toward a direct link between F-actin dynamics and plasma membrane properties at synapses. Importantly, lateral diffusion is likely to contribute to the control of receptor numbers at synapses (Choquet and Triller, 2003; Triller and Choquet, 2005). The data presented here suggest that variations in inhibitory postsynaptic dynamics may have important consequences for the properties of receptor diffusion at synapses.

References

Ackermann M, Matus A (2003) Activity-induced targeting of profilin and stabilization of dendritic spine morphology. Nat Neurosci 6:1194–1200.

Allison DW, Gelfand VI, Spector I, Craig AM (1998) Role of actin in anchoring postsynaptic receptors in cultured hippocampal neurons: differential attachment of NMDA versus AMPA receptors. J Neurosci 18:2423–2436.

Allison DW, Chervin AS, Gelfand VI, Craig AM (2000) Postsynaptic scaffolds of excitatory and inhibitory synapses in hippocampal neurons: maintenance of core components independent of actin filaments and microtubules. J Neurosci 20:4545–4554.

Berridge MJ, Bootman MD, Lipp P (1998) Calcium: a life and death signal. Nature 395:645–648.

Boshart M, Weber F, Jahn G, Dorsch-Hasler K, Fleckenstein B, Schaffner W (1985) A very strong enhancer is located upstream of an immediate early gene of human cytomegalovirus. Cell 41:521–530.

Bresler T, Ramati Y, Zamorano PL, Zhai R, Garner CC, Ziv NE (2001) The dynamics of SAP90/PSD-95 recruitment to new synaptic junctions. Mol Cell Neurosci 18:149–167.

Briggs MW, Sacks DB (2003) IQGAP1 as signal integrator: Ca^{2+}, calmodulin, Cdc42 and the cytoskeleton. FEBS Lett 542:7–11.

Campbell RE, Tour O, Palmer AE, Steinbach PA, Baird GS, Zacharias DA, Tsien RY (2002) A monomeric red fluorescent protein. Proc Natl Acad Sci USA 99:7877–7882.

Carlisle HJ, Kennedy MB (2005) Spine architecture and synaptic plasticity. Trends Neurosci 28:182–187.

Choquet D, Triller A (2003) The role of receptor diffusion in the organization of the postsynaptic membrane. Nat Rev Neurosci 4:251–265.

Colin I, Rostaing P, Triller A (1996) Gephyrin accumulates at specific plasmalemma loci during neuronal maturation in vitro. J Comp Neurol 374:467–479.

Colin I, Rostaing P, Augustin A, Triller A (1998) Localization of components of glycinergic synapses during rat spinal cord development. J Comp Neurol 398:359–372.

Craven SE, El-Husseini AE, Bredt DS (1999) Synaptic targeting of the postsynaptic density protein PSD-95 mediated by lipid and protein motifs. Neuron 22:497–509.

Dahan M, Levi S, Luccardini C, Rostaing P, Riveau B, Triller A (2003) Diffusion dynamics of glycine receptors revealed by single-quantum dot tracking. Science 302:442–445.

Danglot L, Triller A, Bessis A (2003) Association of gephyrin with synaptic and extrasynaptic $GABA_A$ receptors varies during development in cultured hippocampal neurons. Mol Cell Neurosci 23:264–278.

Dillon C, Goda Y (2005) The actin cytoskeleton: integrating form and function at the synapse. Annu Rev Neurosci 28:25–55.

Dosemeci A, Tao-Cheng JH, Vinade L, Winters CA, Pozzo-Miller L, Reese TS (2001) Glutamate-induced transient modification of the postsynaptic density. Proc Natl Acad Sci USA 98:10428–10432.

Dumoulin A, Rostaing P, Bedet C, Levi S, Isambert MF, Henry JP, Triller A, Gasnier B (1999) Presence of the vesicular inhibitory amino acid transporter in GABAergic and glycinergic synaptic terminal boutons. J Cell Sci 112:811–823.

Ebihara T, Kawabata I, Usui S, Sobue K, Okabe S (2003) Synchronized formation and remodeling of postsynaptic densities: long-term visualization of hippocampal neurons expressing postsynaptic density proteins tagged with green fluorescent protein. J Neurosci 23:2170–2181.

Fischer M, Kaech S, Wagner U, Brinkhaus H, Matus A (2000) Glutamate receptors regulate actin-based plasticity in dendritic spines. Nat Neurosci 3:887–894.

Ganeshina O, Berry RW, Petralia RS, Nicholson DA, Geinisman Y (2004) Differences in the expression of AMPA and NMDA receptors between axospinous perforated and nonperforated synapses are related to the configuration and size of postsynaptic densities. J Comp Neurol 468:86–95.

Geinisman Y, Berry RW, Disterhoft JF, Power JM, Van der Zee EA (2001) Associative learning elicits the formation of multiple-synapse boutons. J Neurosci 21:5568–5573.

Giesemann T, Schwarz G, Nawrotzki R, Berhorster K, Rothkegel M, Schluter K, Schrader N, Schindelin H, Mendel RR, Kirsch J, Jockusch BM (2003) Complex formation between the postsynaptic scaffolding protein gephyrin, profilin, and Mena: a possible link to the microfilament system. J Neurosci 23:8330–8339.

Gonzalez-Forero D, Pastor AM, Geiman EJ, Benitez-Temino B, Alvarez FJ

(2005) Regulation of gephyrin cluster size and inhibitory synaptic currents on Renshaw cells by motor axon excitatory inputs. J Neurosci 25:417–429.

Halpain S (2000) Actin and the agile spine: how and why do dendritic spines dance? Trends Neurosci 23:141–146.

Hanus C, Vannier C, Triller A (2004) Intracellular association of glycine receptor with gephyrin increases its plasma membrane accumulation rate. J Neurosci 24:1119–1128.

Harris KM, Jensen FE, Tsao B (1992) Three-dimensional structure of dendritic spines and synapses in rat hippocampus (CA1) at postnatal day 15 and adult ages: implications for the maturation of synaptic physiology and long-term potentiation. J Neurosci 12:2685–2705.

Huang K, El-Husseini A (2005) Modulation of neuronal protein trafficking and function by palmitoylation. Curr Opin Neurobiol 15:527–535.

Inoue A, Okabe S (2003) The dynamic organization of postsynaptic proteins: translocating molecules regulate synaptic function. Curr Opin Neurobiol 13:332–340.

Kennedy MB, Beale HC, Carlisle HJ, Washburn LR (2005) Integration of biochemical signalling in spines. Nat Rev Neurosci 6:423–434.

Kim CH, Lisman JE (1999) A role of actin filament in synaptic transmission and long-term potentiation. J Neurosci 19:4314–4324.

Kirsch J, Betz H (1995) The postsynaptic localization of the glycine receptor-associated protein gephyrin is regulated by the cytoskeleton. J Neurosci 15:4148–4156.

Kirsch J, Betz H (1998) Glycine-receptor activation is required for receptor clustering in spinal neurons. Nature 392:717–720.

Krementsov DN, Krementsova EB, Trybus KM (2004) Myosin V: regulation by calcium, calmodulin, and the tail domain. J Cell Biol 164:877–886.

Krucker T, Siggins GR, Halpain S (2000) Dynamic actin filaments are required for stable long-term potentiation (LTP) in area CA1 of the hippocampus. Proc Natl Acad Sci USA 97:6856–6861.

Kusumi A, Nakada C, Ritchie K, Murase K, Suzuki K, Murakoshi H, Kasai RS, Kondo J, Fujiwara T (2005) Paradigm shift of the plasma membrane concept from the two-dimensional continuum fluid to the partitioned fluid: high-speed single-molecule tracking of membrane molecules. Annu Rev Biophys Biomol Struct 34:351–378.

Langford GM (2002) Myosin-V, a versatile motor for short-range vesicle transport. Traffic 3:859–865.

Levi S, Chesnoy-Marchais D, Sieghart W, Triller A (1999) Synaptic control of glycine and $GABA_A$ receptors and gephyrin expression in cultured motoneurons. J Neurosci 19:7434–7449.

Lissin DV, Gomperts SN, Carroll RC, Christine CW, Kalman D, Kitamura M, Hardy S, Nicoll RA, Malenka RC, von Zastrow M (1998) Activity differentially regulates the surface expression of synaptic AMPA and NMDA glutamate receptors. Proc Natl Acad Sci USA 95:7097–7102.

Maas C, Tagnaouti N, Loebrich S, Behrend B, Lappe-Siefke C, Kneussel M (2006) Neuronal cotransport of glycine receptor and the scaffold protein gephyrin. J Cell Biol 172:441–451.

Marrs GS, Green SH, Dailey ME (2001) Rapid formation and remodeling of postsynaptic densities in developing dendrites. Nat Neurosci 4:1006–1013.

Matsuzaki M, Ellis-Davies GC, Nemoto T, Miyashita Y, Iino M, Kasai H (2001) Dendritic spine geometry is critical for AMPA receptor expression in hippocampal CA1 pyramidal neurons. Nat Neurosci 4:1086–1092.

Matsuzaki M, Honkura N, Ellis-Davies GC, Kasai H (2004) Structural basis of long-term potentiation in single dendritic spines. Nature 429:761–766.

Matus A (2000) Actin-based plasticity in dendritic spines. Science 290:754–758.

McBain CJ, Freund TF, Mody I (1999) Glutamatergic synapses onto hippocampal interneurons: precision timing without lasting plasticity. Trends Neurosci 22:228–235.

Meier J, De Chaldee M, Triller A, Vannier C (2000a) Functional heterogeneity of gephyrins. Mol Cell Neurosci 16:566–577.

Meier J, Meunier-Durmort C, Forest C, Triller A, Vannier C (2000b) Formation of glycine receptor clusters and their accumulation at synapses. J Cell Sci 113:2783–2795.

Meier J, Vannier C, Serge A, Triller A, Choquet D (2001) Fast and reversible trapping of surface glycine receptors by gephyrin. Nat Neurosci 4:253–260.

Meyer G, Kirsch J, Betz H, Langosch D (1995) Identification of a gephyrin binding motif on the glycine receptor beta subunit. Neuron 15:563–572.

Meyer DK, Olenik C, Hofmann F, Barth H, Leemhuis J, Brunig I, Aktories K, Norenberg W (2000) Regulation of somatodendritic $GABA_A$ receptor channels in rat hippocampal neurons: evidence for a role of the small GTPase Rac1. J Neurosci 20:6743–6751.

Mi R, Tang X, Sutter R, Xu D, Worley P, O'Brien RJ (2002) Differing mechanisms for glutamate receptor aggregation on dendritic spines and shafts in cultured hippocampal neurons. J Neurosci 22:7606–7616.

Moss SJ, Smart TG (2001) Constructing inhibitory synapses. Nat Rev Neurosci 2:240–250.

Nagai T, Ibata K, Park ES, Kubota M, Mikoshiba K, Miyawaki A (2002) A variant of yellow fluorescent protein with fast and efficient maturation for cell-biological applications. Nat Biotechnol 20:87–90.

Nicholson DA, Yoshida R, Berry RW, Gallagher M, Geinisman Y (2004) Reduction in size of perforated postsynaptic densities in hippocampal axospinous synapses and age-related spatial learning impairments. J Neurosci 24:7648–7653.

Nusser Z, Lujan R, Laube G, Roberts JD, Molnar E, Somogyi P (1998) Cell type and pathway dependence of synaptic AMPA receptor number and variability in the hippocampus. Neuron 21:545–559.

O'Brien RJ, Mammen AL, Blackshaw S, Ehlers MD, Rothstein JD, Huganir RL (1997) The development of excitatory synapses in cultured spinal neurons. J Neurosci 17:7339–7350.

O'Brien RJ, Kamboj S, Ehlers MD, Rosen KR, Fischbach GD, Huganir RL (1998) Activity-dependent modulation of synaptic AMPA receptor accumulation. Neuron 21:1067–1078.

Oertner TG, Matus A (2005) Calcium regulation of actin dynamics in dendritic spines. Cell Calcium 37:477–482.

Okabe S, Kim HD, Miwa A, Kuriu T, Okado H (1999) Continual remodeling of postsynaptic density and its regulation by synaptic activity. Nat Neurosci 2:804–811.

Okabe S, Urushido T, Konno D, Okado H, Sobue K (2001) Rapid redistribution of the postsynaptic density protein PSD-Zip45 (Homer 1c) and its differential regulation by NMDA receptors and calcium channels. J Neurosci 21:9561–9571.

Okamoto K, Nagai T, Miyawaki A, Hayashi Y (2004) Rapid and persistent modulation of actin dynamics regulates postsynaptic reorganization underlying bidirectional plasticity. Nat Neurosci 7:1104–1112.

Petrini EM, Zacchi P, Barberis A, Mozrzymas JW, Cherubini E (2003) Declusterization of $GABA_A$ receptors affects the kinetic properties of GABAergic currents in cultured hippocampal neurons. J Biol Chem 278:16271–16279.

Prior P, Schmitt B, Grenningloh G, Pribilla I, Multhaup G, Beyreuther K, Maulet Y, Werner P, Langosch D, Kirsch J, Betz H (1992) Primary structure and alternative splice variants of gephyrin, a putative glycine receptor-tubulin linker protein. Neuron 8:1161–1170.

Qian H, Sheetz MP, Elson EL (1991) Single particle tracking. Analysis of diffusion and flow in two-dimensional systems. Biophys J 60:910–921.

Rao A, Kim E, Sheng M, Craig AM (1998) Heterogeneity in the molecular composition of excitatory postsynaptic sites during development of hippocampal neurons in culture. J Neurosci 18:1217–1229.

Richards DA, De Paola V, Caroni P, Gahwiler BH, McKinney RA (2004) AMPA-receptor activation regulates the diffusion of a membrane marker in parallel with dendritic spine motility in the mouse hippocampus. J Physiol (Lond) 558:503–512.

Rose CR, Konnerth A (2001) Stores not just for storage. Intracellular calcium release and synaptic plasticity. Neuron 31:519–522.

Saxton MJ (1993) Lateral diffusion in an archipelago. Single-particle diffusion. Biophys J 64:1766–1780.

Saxton MJ (1997) Single-particle tracking: the distribution of diffusion coefficients. Biophys J 72:1744–1753.

Segal M (2005) Dendritic spines and long-term plasticity. Nat Rev Neurosci 6:277–284.

Seitanidou T, Nicola MA, Triller A, Korn H (1992) Partial glycinergic denervation induces transient changes in the distribution of a glycine receptor-associated protein in a central neuron. J Neurosci 12:116–131.

Sola M, Kneussel M, Heck IS, Betz H, Weissenhorn W (2001) X-ray crystal structure of the trimeric N-terminal domain of gephyrin. J Biol Chem 26:26.

Sola M, Bavro VN, Timmins J, Franz T, Ricard-Blum S, Schoehn G, Ruigrok RW, Paarmann I, Saiyed T, O'Sullivan GA, Schmitt B, Betz H, Weissenhorn W (2004) Structural basis of dynamic glycine receptor clustering by gephyrin. EMBO J 23:2510–2519.

Star EN, Kwiatkowski DJ, Murthy VN (2002) Rapid turnover of actin in dendritic spines and its regulation by activity. Nat Neurosci 5:239–246.

Thery M, Racine V, Pepin A, Piel M, Chen Y, Sibarita JB, Bornens M (2005) The extracellular matrix guides the orientation of the cell division axis. Nat Cell Biol 7:947–953.

Toni N, Buchs PA, Nikonenko I, Bron CR, Muller D (1999) LTP promotes formation of multiple spine synapses between a single axon terminal and a dendrite. Nature 402:421–425.

Toni N, Buchs PA, Nikonenko I, Povilaitite P, Parisi L, Muller D (2001) Remodeling of synaptic membranes after induction of long-term potentiation. J Neurosci 21:6245–6251.

Triller A, Choquet D (2005) Surface trafficking of receptors between synaptic and extrasynaptic membranes: and yet they do move! Trends Neurosci 28:133–139.

Watanabe T, Noritake J, Kaibuchi K (2005) Regulation of microtubules in cell migration. Trends Cell Biol 15:76–83.

Zhang W, Vazquez L, Apperson M, Kennedy MB (1999) Citron binds to PSD-95 at glutamatergic synapses on inhibitory neurons in the hippocampus. J Neurosci 19:96–108.

Zheng JQ (2000) Turning of nerve growth cones induced by localized increases in intracellular calcium ions. Nature 403:89–93.

Zhou Q, Xiao M, Nicoll RA (2001) Contribution of cytoskeleton to the internalization of AMPA receptors. Proc Natl Acad Sci USA 98:1261–1266.

van Zundert B, Alvarez FJ, Yevenes GE, Carcamo JG, Vera JC, Aguayo LG (2002) Glycine receptors involved in synaptic transmission are selectively regulated by the cytoskeleton in mouse spinal neurons. J Neurophysiol 87:640–644.

van Zundert B, Alvarez FJ, Tapia JC, Yeh HH, Diaz E, Aguayo LG (2004) Developmental-dependent action of microtubule depolymerization on the function and structure of synaptic glycine receptor clusters in spinal neurons. J Neurophysiol 91:1036–1049.